International Journal of Material Forming (2025) 18:44
https://doi.org/10.1007/s12289-025-01906-7

ORIGINAL RESEARCH

Metamodel-based control algorithms for the correction of bending angle after springback in an industrial U-Bending process

L. Muñiz[1] · L. Galdos[1] · J. Trinidad[1]

Received: 7 June 2024 / Accepted: 12 April 2025

Abstract
The increased complexity of geometries and the improved properties of sheet metal components result in narrower process windows, highlighting the need for better process control to minimize deviations and to ensure the production of high-quality parts. In this context, this study focuses on controlling the bending angle of a seat rail component manufactured by a renowned TIER1 company. This angle changes due to material, process fluctuations and post-forming springback. Two types of material, a cold-rolled Dual Phase DP980 steel and a Complex Phase CP980 high-strength steel, are both employed interchangeably when manufacturing this component. Variations in the mechanical properties and thickness of these two materials result in significant differences in post-springback bending angle. To tackle this challenge, various control strategies have been developed including a classical controller and a controller enhanced with a metamodel-based feedforward term. For the latter, two approaches were used: a simulation-based metamodel and an experimental data-based metamodel. Heuristic-based disturbances, reflecting both material variability and process changes (tool mounting variations, tool wear, gap changes and temperature variations), have been considered. To calibrate the new controller parameters and gains, a constrained-based genetic algorithm approach has been utilized together with a numerical virtualization of the process. After this virtual set-up, the new controllers have been tested experimentally in a real environment, using an industrial U-bending tool and a 4000 kN servomechanical press. The new controllers have proven to be an efficient method for enhancing the process robustness. A classical controller, employing a feedback control system, enabled consideration of part-to-part variations. On the other hand, the addition of a metamodel-based feedforward term facilitated anticipation of material properties and sheet thickness changes, thereby preventing scrap production.

Keywords U-bending · Control · Feedback · Feedforward · Metamodeling

Introduction

Global industry currently produces 200 kg of steel [1] and 7 kg of aluminum [2] per person per year, and transforms this into a wide range of products, from vehicles to final goods at an unprecedentedly low cost. Given the substantial amount of raw materials consumed by modern civilization, there is a growing demand for the transition to more sustainable and energy-efficient production systems. Consequently, companies are under increasing pressure to achieve zero defects in manufacturing. This objective is gradually being realized through the adoption of Industry 4.0 approaches, made possible by the enhanced computational capacity and faster electronics available in industry.

The increasing complexity of sheet metal forming components and the stringent tolerances required by the market have forced the manufacturing industry to devise new strategies to operate within the available process window. In this context, the development of new process monitoring systems and control strategies is crucial for promptly adjusting process parameters and ensuring the production of defect-free components.

In order for a process to be controllable, part quality indicators need to be both detectable and measurable. Additionally, these indicators must be modifiable through another process variable, for example an actuator. The process adjustment can be made manually using operator expertise or automatically, using advanced controllers and expert systems.

✉ L. Muñiz
lmuniz@mondragon.edu

[1] Department of Mechanical and Industrial Production, Mondragon Unibertsitatea, Loramendi 4, 20500 Mondragon, Gipuzkoa, Spain

Published online: 05 May 2025

Regarding quality indicators, some typical defects in sheet metal forming processes are thinning, splitting, wrinkling and springback. In bending processes, which are the focus of this paper, springback is the main problem [3–6]. Springback depends on several process variables [7], such as material properties (sheet thickness, yield strength, etc.) and tool and process parameters (speed, lubrication, temperature, etc.). In this regard, process fluctuations are the biggest obstacles to effectively controlling a metal bending process. The most typical process fluctuations and uncertainties in cold forming can include changes in material properties and thickness, tool temperature evolution during production, and tool wear.

Initial material properties can influence final properties, such as geometry, surface finishing, and residual stresses. Harsch et al. [8] tested the same material (stainless steel 1.4301) from different suppliers to analyze fluctuations of material properties, as these often lead to robustness problems in production. They found significant differences between suppliers. The authors defined this material changes as process noise, or more specifically, as repeatability uncertainties, as they are often non-measurable. Authors from the same research group at ETH Zurich demonstrated that there are significant fluctuations in material properties between different batches and suppliers, as well as in sheet thicknesses [9, 10]. This type of fluctuations significantly affects the final U-bending angle after springback.

In [11], Muñiz et al. analyzed the mechanical and microstructural fluctuations of five different high-strength steels used in the production of the industrial demonstrator that is used in this study. They examined the impact of these fluctuations on the bending angle after springback. The study found variations of up to 0.65º in the bending angle between batches from the same material supplier under the same process parameters, and variations of up to 1.25º between batches from different suppliers.

For these reasons, and to avoid producing scrap and achieve zero-defect manufacturing, advanced real-time part-to-part control algorithms are necessary. These algorithms can adjust the bending process to ensure that production remains within the desired tolerance window. The variables that can be adjusted to influence the quality indicators and final product dimensions are known as control variables [12–15, 15, 15–23, 23–27].

In several studies, punch displacement is the primary control variable [12–18]. In some of them, punch force provides feedback for corrections [12–14, 17, 19, 20]. Additionally, other press variables and tool dimensions have been employed as control variables, including punch radius [15, 21–23], die opening [23–25], and tool angle [26], in terms of batch-to-batch control, and punch speed [15] and binder force [27], among others.

Regarding advanced controllers for metal forming and deep drawing, various types of control systems have been developed, both for in-line use and utilizing post-process database information. The most recent developments range from classical controllers [28, 29] to modern metamodel-based controllers [30–34] and a new branch of control systems that use machine learning techniques for process control [35–37]. In terms of tuning feedback controllers for metal forming applications, Endelt et al. [38] developed a feedback controller where the gain factors of the control loop were determined by solving an optimal control problem formulated as a non-linear least-squares minimization task.

Like in metal forming and deep drawing, various algorithms have been utilized to control springback in bending. These include fuzzy logic [19, 22], Artificial Neural Networks (ANN) [20, 21, 24, 25, 36, 39, 40], analytical models [41–43], analytical models derived from FEM analysis combined with neural networks [25], Kriging metamodels [27, 44], regression models [15, 16, 45], genetic algorithms combined with neural networks [23], PI controllers [27], and a simple online punch force database [19], among others. To identify the most influential process parameters affecting springback suitable for process control, different authors have employed FEM along with Taguchi and analysis of variance (ANOVA) methods [46, 47].

While simple classical controllers with a feedback term are often suitable for serial production, there is a noticeable trend toward the adoption of metamodel-based controllers. These controllers can take unexpected process variations into account and predict optimal process variables to produce a quality component, as they incorporate physical information into their development process. For instance, a classical controller lacks the ability to anticipate material fluctuations, unlike a model-based controller that is equipped with a feedforward term capable of incorporating material property information. Similarly, a classical controller cannot consider the cooling of tools and its impact when production stops (due to failure downtime or factory rest time). Conversely, an advanced controller could predict the new optimal process setting if the metamodel integrated into the controller includes information about the tool temperature, possibly obtained through a temperature sensor. This unique feature is increasingly demanded by industries, especially as production batches become smaller and the need for scrap reduction and the creation of more sustainable processes grows.

This work introduces modern controllers designed to control the bending angle after springback of a seat rail component manufactured by a TIER1 company. The production of the selected component utilizes either cold-rolled DP980 or CP980 high-strength steels, depending on material availability and other economic factors. As demonstrated by the authors in [11], material fluctuations result in significant variability in the final bending angle

of this component. To address this challenge, two different control strategies have been developed and tested: i) a classical controller using Proportional-Integral (PI) terms and ii) an advanced controller that combines a classical controller with a metamodel-based feedforward term. In the latter, two types of metamodels have been utilized: a simulation-based metamodel and an experimental data-based metamodel.

Heuristic-based disturbances, reflecting material variability and long-term machine variations occurring during production, have been taken into account during the development of the controllers. To assess the robustness of the controllers and to train them, various scenarios have been simulated using a virtual environment. Finally, after tuning the control parameters, the three types of controllers (the classical PI controller and the two metamodel-based controllers) have been tested in a 400 kN industrial servo-mechanical press using industrial tooling and in-situ bending measurement sensors.

Process metamodeling using FEM

Material characterization and modeling

Aiming to develop a FEM-based metamodel of the U-bending process to be embedded in the advanced controller, which combines a classical controller with a metamodel-based feedforward term, a numerical model has been created using ABAQUS 6.14.

For this purpose, five materials have been studied: three DP980 Dual Phase steels and two CP980 Complex Phase steels, sourced from three different suppliers. The materials are named as follows:

- DP980 1 and DP980 2: supplier 1, different batches
- DP980 3: supplier 2
- CP980 1 and CP980 2: supplier 3, different batches

The principal mechanical properties of the five materials obtained through uniaxial tensile tests are summarized in Table 1. For more details, please refer to [11].

The material hardening of the DP980 and CP980 materials has been modelled using the Swift Hockett-Sherby law (Eq. (1)) [48], as it is demonstrated to be one of the best suited hardening models for this type of materials [49]. For the initial experimental extrapolation of the curves, the small area technique available in GOM Aramis software was used [49].

$$\sigma = (1-\alpha)\left\{C * \left(\varepsilon_{pl}+\varepsilon_0\right)^m\right\} + \alpha\left\{\sigma_{\mathrm{Sat}} - \left(\sigma_{\mathrm{Sat}}-\sigma_i\right)e^{-a\varepsilon_{pl}^p}\right\} \quad (1)$$

Table 1 Main mechanical properties and average sheet thicknesses of the five materials, analyzed at rolling direction

Material	$R_{p0.2\%}$ [MPa]	UTS [MPa]	n [-]	r_n [-]	Elongation [%]
DP980 1	883.7	1085.6	0.045	0.96	9.2
DP980 2	875.9	1078.1	0.05	0.98	9.7
DP980 3	852.1	1041.8	0.049	0.95	11.7
CP980 1	916.7	1009.6	0.037	0.91	10.8
CP980 2	865.5	966.3	0.048	0.93	12.1

where a m, and p are material exponents in the Swift-Hockett Sherby hardening law, ε_0 is the pre-strain, σ_i is the initial stress, σ_{Sat} is the saturation stress, α is the weighting factor between Swift and Hockett-Sherby models, and C is a coefficient in the Swift-Hockett Sherby hardening law [50, 51]. To account for material fluctuations, three different virtual hardening laws have been developed, reflecting the real variability of the materials. First, an average curve was created from the data of the five materials to define a baseline hardening law. Then, variations were introduced by adjusting this curve by ± the Ultimate Tensile Strength (UTS). This resulted in three distinct hardening laws: one using a low UTS, one with an intermediate UTS, and one with a high UTS. The measured hardening curves of the five materials coming from three different suppliers and the virtual hardening laws are shown in Fig. 1a and b. Table 2 lists all parameter values for the expression in Eq. (1).

A Von Mises yield criterion has been chosen to model the material. As shown in Table 1, all the materials exhibited a normal anisotropy between 0.91 and 0.98. Given that the bending operation follows a plane strain condition, the differences between an anisotropic and an isotropic yield criterion have been minimal.

Finite Element Modeling

The U-bending process numerical model has been created with static-general implicit analysis (ABAQUS Standard 6.14). Due to the symmetry of the component, only one half has been simulated to reduce computational time. The final model developed is shown in Fig. 2.

The punch and die have been modelled as analytical rigid surfaces, while the blank material has been meshed using CPE8R finite element.. The mesh size was selected based on a mesh size sensitivity analysis, where the number of elements through the thickness was varied. The analysis showed that using 75 elements through the thickness in the bending zone provided an optimal balance between computational time and model accuracy.

For the definition of the coefficient of friction, strip drawing tests were performed using a servo-mechanical tester [52]

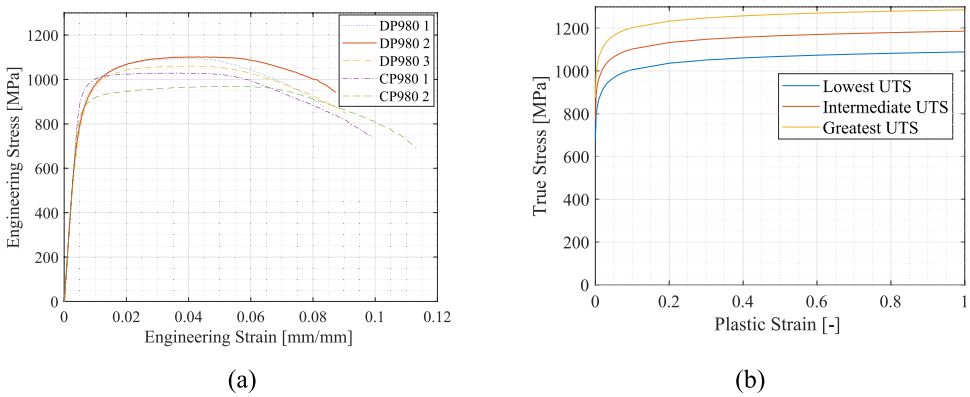

(a) (b)

Fig. 1 (**a**) Engineering stress–strain curves of the five materials and (**b**) hardening curves of the materials analyzed

Table 2 Swift and Hockett–Sherby model parameters for the intermediate UTS hardening law

Parameter	α	C [MPa]	ε_0	m	σ_{Sat} [MPa]	σ_i [MPa]	a	p
Value	0.25	1173.8	0.00739	0.0336	1295.7	185.7	7.284	0.4402

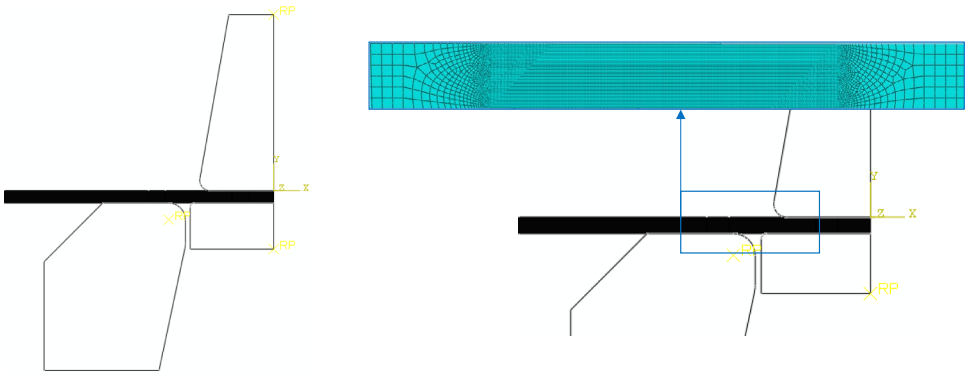

(a) (b)

Fig. 2 (**a**) U-bending process model and (**b**) mesh configuration scheme of the sheet and zoom of the finer mesh in the bent zone

and the as-received precuts in the pre-oiled condition. Finite element results indicate that during the bending process, sliding velocity varies from 400 mm/s to 0 mm/s. Therefore, strip drawing tests were conducted at 10 mm/s and 50 mm/s with contact pressures up to 50 MPa (the maximum reachable in the experimental setup used for this work). A Filzek-type friction law (see Eq. (2)) [53], which depends on contact pressure and sliding velocity, was then fitted to the experimental friction coefficients measured in the strip drawing tests:

$$\mu_{\text{eff}} = \mu\left(\frac{p}{p_{\text{ref}}}\right)^{e-1} - a \cdot \ln\left(\frac{max\left(v_{\text{rel}}, v_{\text{ref}}\right)}{v_{\text{ref}}}\right) \tag{2}$$

where μ is the base friction coefficient, p is the contact pressure, p_{ref} is the reference pressure, e is the pressure exponent, a is the velocity factor, v_{rel} is the velocity of the sheet relative to the tool in contact and v_{ref} is the reference velocity. The experimental values of the friction coefficient and the fitted friction law are shown in Fig. 3. The coefficients are shown in Table 3.

To test the assumption that differences between anisotropic and isotropic models are minimal, a 3D model with the Hill criterion was compared to a 2D model with the Von Mises criterion. An absolute difference of 0.43° was found between the 3D and 2D models. Therefore, considering the reduction in computational cost when using a 2D model and the small difference between the two models, the Von Mises yield criterion was used in this work.

A summary of the numerical model is detailed in Table 4.

Numerical metamodel

As demonstrated by the authors in [11] through a correlation analysis carried out, the press stroke is the most influential factor on the bend angle after springback. Following this, sheet thickness and Ultimate Tensile Strength (UTS) also

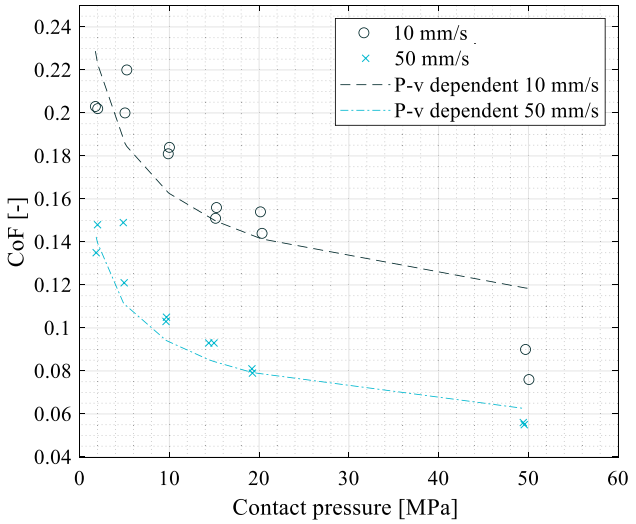

Fig. 3 Experimental friction coefficients and fitted Filzek friction law

Table 3 Coefficients of the Filzek pressure and velocity dependent law

Coefficient	Pressure exponent (e)	Velocity factor (a)	p_{ref} [MPa]	v_{ref} [mm/s]
Value	0.8470	0.0255	2	4.7734

have a significant impact. For this reason, these process parameters and their fluctuations have been considered in the development of the metamodels.

The punch stroke is the parameter that defines the final bending angle before springback. As depicted in Fig. 4a, initially, the punch bends the precut material. Subsequently, as the punch traverses the die radius and die flat vertical zones, two lateral cams are closed using the punch movement to overbend the sheet (see Fig. 4b). Finally, springback occurs, and the final post-springback angle (α) is the variable that needs to be controlled in the process (Fig. 4c). Note that a larger α indicates a lower springback of the product. The initial distance between the punch and the cams is referred to as the gap. The coordinates of two nodes of the part in the numerical model are used to calculate the post springback bending angle, applying the same procedure described later for the experimental measurements in Fig. 6b.

Table 4 Numerical model parameters

Parameter	Type/value
Element type	Quadratic quadrilateral CPE8R
Number of elements	32258
Layers through thickness	Global: 6, Bending zone: 75
Mesh size	Global: 0.25 mm, Bending zone: 0.02 mm
Solver	Abaqus Standard 6.14
Hardening model	Swift-Hockett-Sherby (Eq. (1))
Young Modulus	205 GPa
Poisson's ratio	0.3
Yield Criteria	Von Mises with associated flow rule
Friction coefficient	Filzek law (pressure and velocity dependent)
Computation time	17811 s

A full-factorial design [54, 55] with a central point has been developed using Minitab commercial software. The four main factors are: the punch stroke or press position (with three levels); the gap between the tool and die (with two levels); the sheet thickness (with three levels); and the ultimate tensile strength (UTS) (with three levels). The variable limits have been chosen based on tensile tests for the material properties, thickness measurements in the real precuts, and cams manufacturing and assembly tolerances. A total of 55 simulations have been carried out. Table 5 outlines the parameters and their ranges used in the variant simulations.

For the metamodeling, Response Surface Methodology (RSM) [56] obtained through Minitab software has been selected. Among different metamodeling techniques, RSM is well-established, easy to use, best suited for applications with random error, and appropriate for applications with fewer than 10 factors [57]. It relies on the assumption that many physical systems are smooth and continuous, making them well-approximated by low-order polynomials, especially within the region of interest. In this work, a second-order model (Eq. (3)) with interactions has been employed:

$$y = \beta_0 + \sum_{j=1}^{k} \beta_j x_j + \sum_{j=1}^{k} \beta_{jj} x_j^2 + \sum_{i<j=2}^{k} \beta_{ij} x_i x_j \tag{3}$$

where β_0, β_j, β_{jj} and β_{ij} are regression coefficients, x_j are independent variables, and y is the response, in this case, the bending angle after springback. The equation is shown below:

$$\begin{aligned}\alpha_n = {} & -0.1584 \cdot gap^2 - 3.29 \times 10^{-5} \cdot gap \cdot UTS - 0.1124 \cdot \text{ gap } \cdot \text{ Stroke } - 0.2749 \cdot \text{ gap } \cdot t + 1.8213 \cdot gap \\ & - 9.05 \times 10^{-8} \cdot UTS^2 - 2.15 \times 10^{-6} \cdot UTS \cdot \text{ Stroke } - 3.96 \times 10^{-5} \cdot UTS \cdot t + 0.000284 \cdot UTS \\ & + 0.00916 \cdot \text{ Stroke }^2 + 0.1445 \cdot \text{ Stroke } \cdot t - 0.1450 \cdot \text{ Stroke } + 0.9265 \cdot t^2 - 3.3597 \cdot t + 2.1912\end{aligned} \tag{4}$$

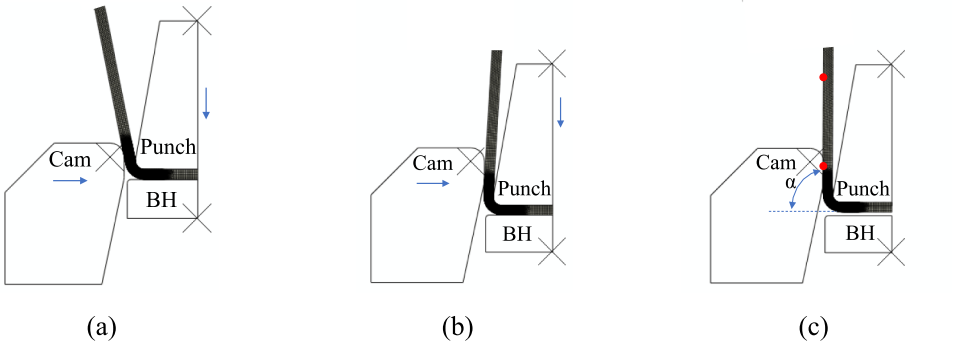

Fig. 4 U-bending tool kinematics. (**a**) initial bending step, (**b**) overbending using cams and (**c**) final stage after springback. BH refers to blank-holder. Red circles denote nodes location for angle measurement, and blue arrows denote punch and cams displacement direction

Table 5 Input parameters and their variations for U-bending modeling

Parameter	Lower limit	Nominal	Upper limit
Punch stroke or x [mm]	10	10.5	11
Blank thickness t [mm]	1.45	1.5	1.55
Gap between tool and die [mm]	1.5	1.55	1.6
UTS [MPa]	925.71	1025.71	1125.71

Table 6 Error metrics of the numerical metamodel developed with the Response Surface Methodology

R-squared [-]	RMSE [°]	MAE [°]
0.98	0.31	0.25

where Stroke, *UTS*, *gap*, and t are the press stroke, ultimate tensile strength, gap, and sheet thickness respectively. α_n is the standardized post-springback bending angle, obtained by dividing the angle by the objective bending angle, with standardized values ranging from 0.957 to 1.128. To evaluate the accuracy of the metamodel, three error metrics have been used: i) the *R*-squared (Eq. (5)), ii) the Root Mean Squared Error (MSE) (Eq. (6)) and iii) the Mean Average Error (MAE) (Eq. (7)) [58].

$$R^2 = 1 - \frac{\sum_i \left(y_i' - y_i\right)^2}{\sum_i \left(y_i - \bar{y}_i\right)^2} \tag{5}$$

$$RMSE = \sqrt{\sum_{i=1}^{n} \frac{\left(y_i' - y_i\right)^2}{n}} \tag{6}$$

$$MAE = \frac{\sum_{i=1}^{n} \left|y_i - y_i'\right|}{n} \tag{7}$$

where y' denotes the predicted value of the i-th part; y represents the experimental value for the experimental metamodel and the value derived from numerical simulations for the numerical metamodel; n is the total number of observations, and $\bar{y}$ is the mean value of the data.

Table 6 presents the error metrics obtained for the numerical metamodel.

Figure 5a illustrates the predicted bending angle after springback versus the bending angle obtained through simulation using the created FEM model. As indicated by the error metrics, there is an acceptable correlation. In Fig. 5b, the correlation between the bending angle after springback and the analyzed variables is shown.

Process metamodeling using experimental bending measurements

The development of advanced controllers using FEM-based metamodels is highly desirable in an industrial environment. This approach allows for the creation of advanced controllers without generating a large number of defective parts and scrap. Additionally, it offers the advantage of enabling the testing of various virtual scenarios, which may not be feasible in the real world (for example, due to unattainable specific material properties or inability to achieve a specific thickness).

However, numerical metamodels also have several limitations. In our case study, which involves the bending process at industrial production rates, it is challenging to consider long-term effects such as tool heating, tool wear, press deterioration, etc., or explicit process variations caused by erroneous tool mounting, tool misalignment, etc.

For this reason, and to compare the results obtained using an advanced controller that combines a classical controller with a metamodel-based feedforward term constructed solely with numerical results and experimental ones, an extensive experimental bending campaign was launched. The purpose was to create an experimental database and develop a metamodel using real bending measurements, hereafter called the experimental metamodel.

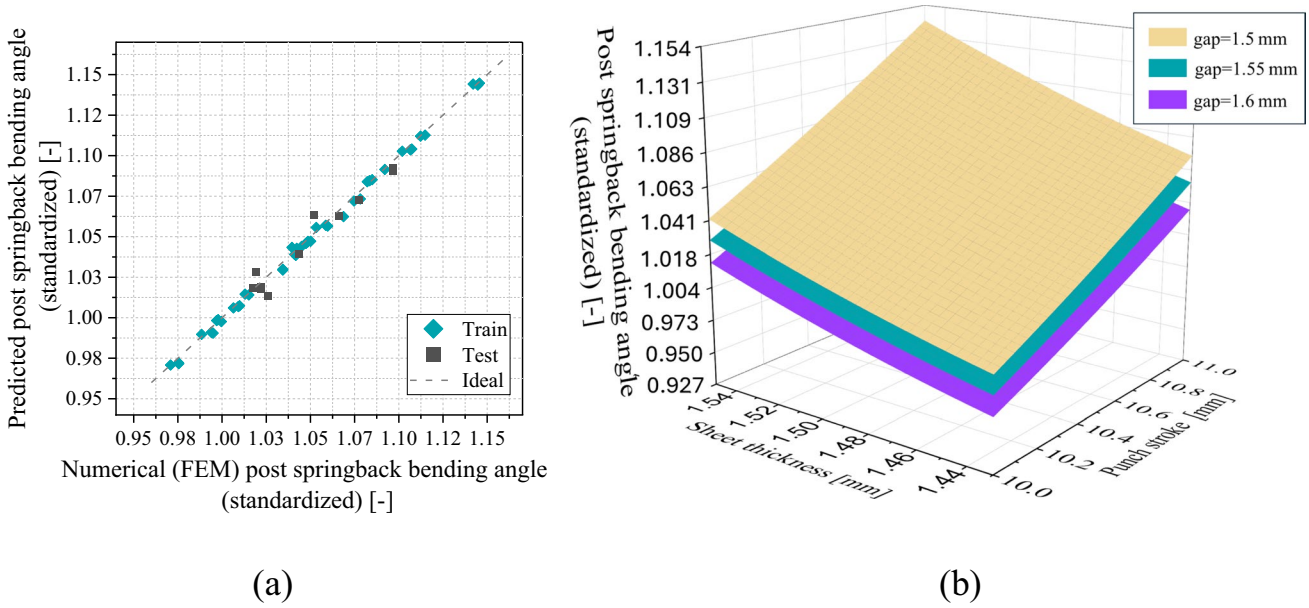

Fig. 5 (**a**) Metamodel prediction vs numerical (FEM) bending angle after springback. Values are standardized in respect to the optimal angle and are therefore dimensionless. (**b**) a 3D plot of bending angle after springback vs. press stroke and sheet thickness for three different gap values and a nominal UTS of 1025.71 MPa

Table 7 Variation of input parameters in the experimental tests

Parameter	Lower limit	Upper limit
Punch stroke [mm]	10.76	11.17
Blank thickness [mm]	1.43	1.52
Ultimate Tensile Strength UTS [MPa]	966.3	1085.6

The experimental tests involved 10 repetitions per material for five different press strokes, totaling 250 parts tested. For each part, the bending angle after springback, sheet thickness, and press stroke were measured The UTS values obtained from tensile testing (Table 1) were used as input for the controllers. Limits of the input variables are detailed in Table 7.

The press velocity was 32 spm for all parts. To measure the experimental bending angle, a measuring tool comprising two Linear Variable Differential Transformers (LVDTs) was developed (Fig. 6a). The bend angle was calculated based on the vertical and horizontal positions of the transducers (Fig. 6b). The device has an accuracy of $\pm 0.08°$ and is shown in Fig. 6c.

Table 8 shows the average sheet thickness measured in-line for each CP980 and DP980 analyzed. The standardized bending angle after springback versus the punch stroke is shown in Fig. 7.

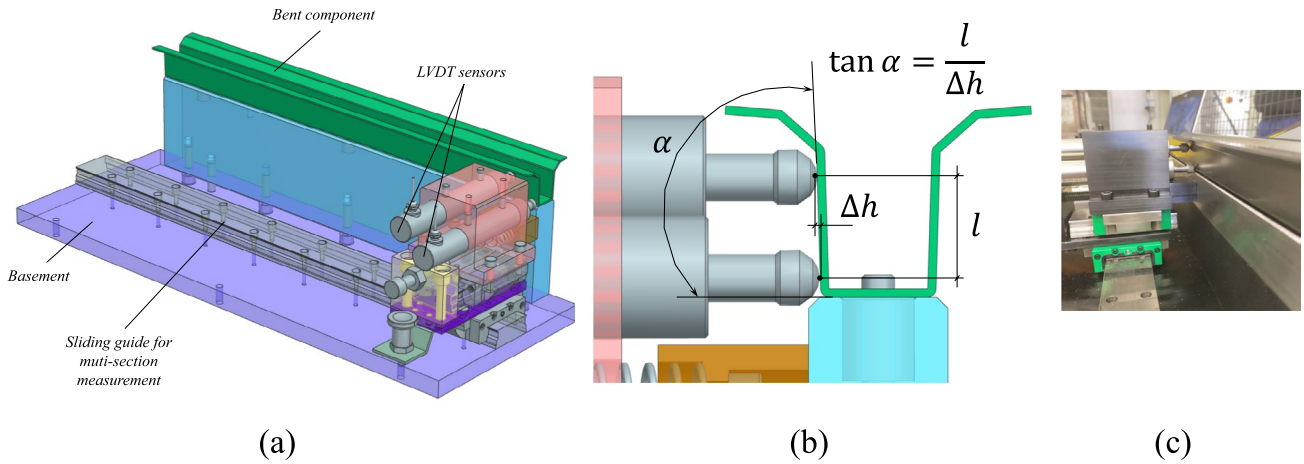

Fig. 6 Measuring tool for angle measurement. (**a**) CAD design, (**b**) schematic for angle calculation and (**c**) real tool

Table 8 Average sheet thickness of the 250 specimens analyzed

Material	DP980 1	DP980 2	DP980 3	CP980 1	CP980 2
Sheet thickness [mm]	1.46	1.49	1.49	1.50	1.49

Table 9 Error metrics of the experimental metamodel developed using Response Surface Methodology

R-squared [-]	RMSE [°]	MAE [°]
0.96	0.134	0.110

The experimental metamodel, has been generated using the same methodology as in the numerical case, using a second-order model with interactions.. After preprocessing the data, the model was trained, tested, and validated. Eighty percent of the data was selected for training, while the remaining twenty percent was used for testing. Equation (8) is as follows:

$$\begin{aligned}\alpha_n = {} & 1.6855 - 0.1380 \cdot \text{Stroke} - 0.00033 \cdot UTS - 0.0158 \cdot t + 0.00847 \cdot Stroke^2 \\ & - 3.39 \times 10^{-8} \cdot UTS^2 - 0.0407 \cdot t^2 + 2.60 \times 10^{-6} \cdot \text{Stroke} \cdot UTS \\ & - 0.00305 \cdot Stroke \cdot t + 0.00021 \cdot UTS \cdot t \end{aligned} \tag{8}$$

where Stroke, UTS, and t are the punch stroke, ultimate tensile strength, and sheet thickness respectively, and α_n is the normalized post-springback bending angle, standardized by dividing the angle value by the objective bending angle.

The error metrics obtained for the experimental metamodel are shown in Table 9, indicating an acceptable correlation.

Figure 8 illustrates the predicted bending angle after springback versus the bending angle obtained experimentally using the created experimental metamodel for the 250 parts produced in the forming press.

Numerical-experimental metamodel comparison

The difference between the numerical and the experimental metamodels can be observed in Fig. 9. The numerical metamodel proved to be more sensitive to changes in both stroke and sheet thickness, showing a more pronounced slope. The numerical metamodel predicts higher post springback bending angles for the same press strokes. These differences could be put down to the elastic deflection of the tools, the gap differences between the numerical and the experimental case, and possible temperature effects.

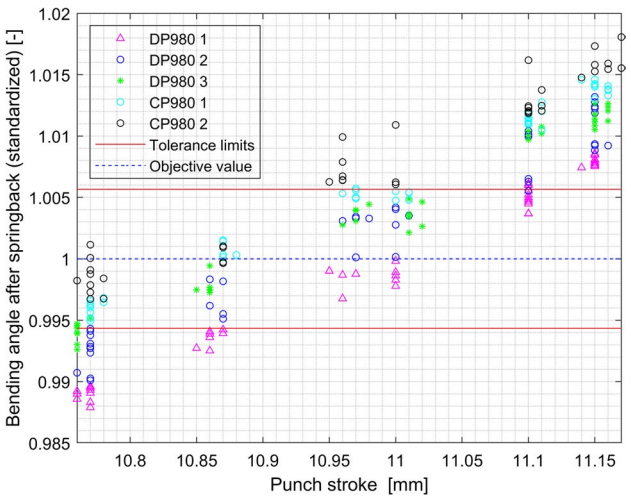

Fig. 7 Bending angle after springback (standardized) vs punch stroke for the different materials

Advanced controllers and virtual tuning of parameters

U-Bending controllers

As mentioned before, three different controllers have been developed and tested using industrial tooling and an industrial environment, with a 400 kN press. The control variable is the punch stroke, and disturbances reflecting material and process variability were introduced in the controllers as random variations, explained in Sect. 5.2. The three main controllers are explained in the next sections.

Feedback controller with proportional-integral (PI) terms (FB controller) Firstly, a simple feedback controller that utilizes the measurements of the bending angle after springback for the i-th part ($\alpha(i)$) to determine the press stroke for the subsequent part ($x(i+1)$) has been defined. The objective of the controller is to minimize the difference between the desired angle and the experimentally measured angle. The feedback controller is depicted in Fig. 10. Note that inherent process disturbances are decoupled from the bending process intentionally. This is done as virtual disturbances have been used to tune the controllers' gains.

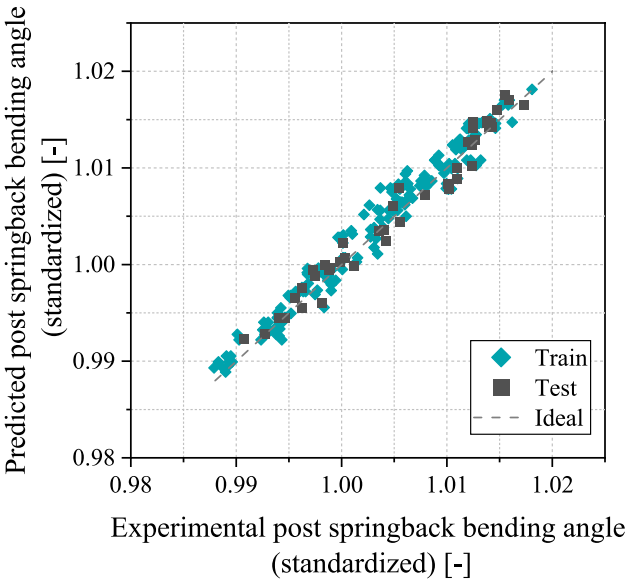

Fig. 8 Predicted with the experimental metamodel vs. experimental bending angle after springback. Values are standardized in respect to the optimal angle

The feedback error $e(i)$ is defined as the difference between the bend angle after springback of each sample $\alpha(i)$ and the target bend angle after springback α_{REF} (Eq. (9)):

$$e(i) = \alpha(i) - \alpha_{REF} \tag{9}$$

The stroke of the current part $x(i)$ is given by Eq. (10)

$$x(i) = x(i-1) + \Delta x(i) \tag{10}$$

where $x(i-1)$ is the previous stroke and $\Delta x(i)$ is the variation in press stroke of the current part, given by Eq. (11)

$$\Delta x(i) = K_p \cdot e(i-1) + K_I \cdot \sum_{j=1}^{i-1} e(j) \tag{11}$$

where K_p and K_I are the proportional and integral gains of the controller, respectively. These gains have been adjusted using constrained genetic algorithm optimization, as will be explained later. With this global optimization approach, we avoid getting stuck in local minima. Another strategies as grid or local search could be also appropriate for this task. No derivative action is used in the controller because strong part-to-part variation reduces the stability of the controller. Note that this simple and classical controller is unable to account for material and thickness fluctuations effects.

Feedforward + Feedback controller with proportional-integral (PI) terms – numerical metamodel (FF + FB Numerical controller) Secondly, an advanced controller, combining feedback and feedforward terms, has been developed. The feedback

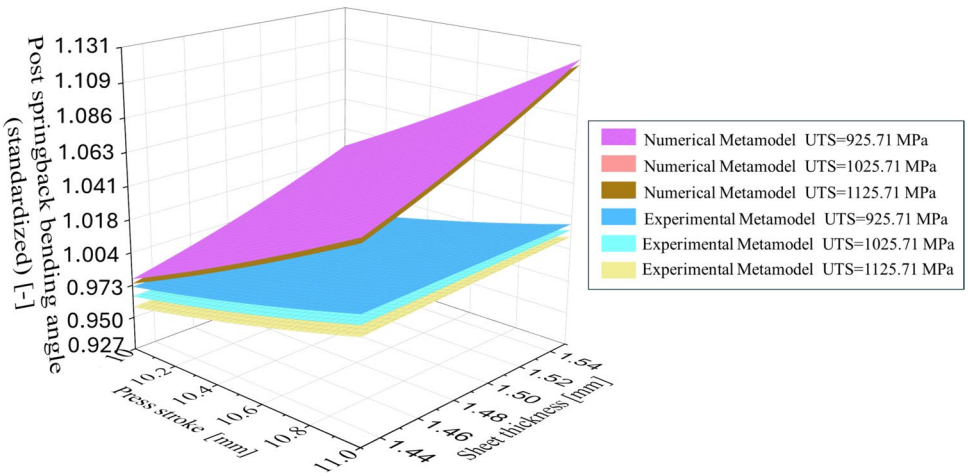

Fig. 9 A 3D plot of post springback bending angle vs. press stroke and sheet thickness comparing the numerical and the experimental metamodel for three UTS levels: 925.71 MPa, 1025.71 MPa and 1125.71 MPa. An intermedium gap of 1.55 mm was selected for the numerical response surface plots

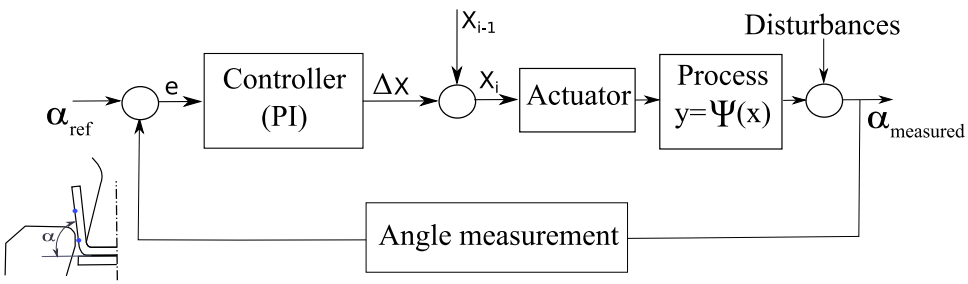

Fig. 10 Feedback (FB) control scheme with a proportional controller

controller solely minimizes differences between the last part and a reference, relying on previously produced parts. In contrast, feedforward control is a physics-based model or a metamodel that anticipates optimal strokes for forthcoming material properties. However, the feedforward controller is not able to react to non-measurable influences, such as tool heating. Therefore, a feedback loop in combination with the feedforward term is desirable to adjust the optimal stroke by considering unexpected disturbances. This integrated approach enables the controller to adaptively respond to both known and unknown sources of variation, enhancing the robustness and effectiveness of the control system.

With this aim, a hybrid controller has been designed, where the feedforward term is governed by the numerical metamodel created using FEM simulations as explained in Sect. 2, and the feedback term is controlled with a Proportional-Integral (PI) controller. The proportional term brings the instantaneous error close to zero, while the integral term decreases the steady-state error caused by external disturbances, considering the accumulated error over time. This combined approach combines the predictive capabilities of the feedforward term based on the numerical metamodel, along with the adaptive nature of the feedback term provided by the PI controller.

Figure 11 illustrates the main structure of the feedback and feedforward control scheme. As in the previous case, note that inherent process disturbances are decoupled from the bending process intentionally. This is done as virtual disturbances have been used to tune the controllers' gains.

In the proposed controller, Δx_{FB} determines the new punch stroke considering part-to-part-and cumulative error using the PI controller. Variation in press stroke is obtained as shown in Eq. (12):

$$\Delta x_{FB}(i) = K_p \cdot e(i-1) + K_I \cdot \sum_{j=1}^{i-1} e(j) \tag{12}$$

where K_p and K_I are the proportional and integral gains, calculated using constrained genetic algorithm optimization, as for the purely feedback controller.

The feedforward term provides the optimal punch stroke considering the forthcoming material properties and sheet thickness of the part before bending using the numerical metamodel.

$$x_{FF}(i) = f(t(i), UTS(i)) \tag{13}$$

The optimal punch stroke is the sum of the optimal punch stroke x_{FF} and the correction provided by the feedback controller Δx_{FB} (Eq. (14)):

$$x(i) = x_{FF}(i) + \Delta x_{FB}(i) \tag{14}$$

Feedforward + feedback controller with proportional-integral (PI) terms – experimental metamodel (FF + FB Experimental controller) Thirdly, the second hybrid controller was duplicated with the only change being that the feedforward term is governed by the experimental metamodel, as explained in Sect. 3. This metamodel has been developed using real bending experiments with the five materials, and thus, it is expected to be the most accurate of all the models.

Virtual testing and tuning of controllers

In order to test and tune the proposed control algorithms before deploying them in the industrial environment, a virtual testing environment has been created where different scenarios have been evaluated. The bending process has been virtualized using the experimental metamodel, as this most accurately reflects the real environment that needs to be controlled.

Because the bending angle after springback fluctuates for the same process variables due to non-controllable disturbances, the variability observed experimentally (see Fig. 7) has been introduced with a random distribution in the

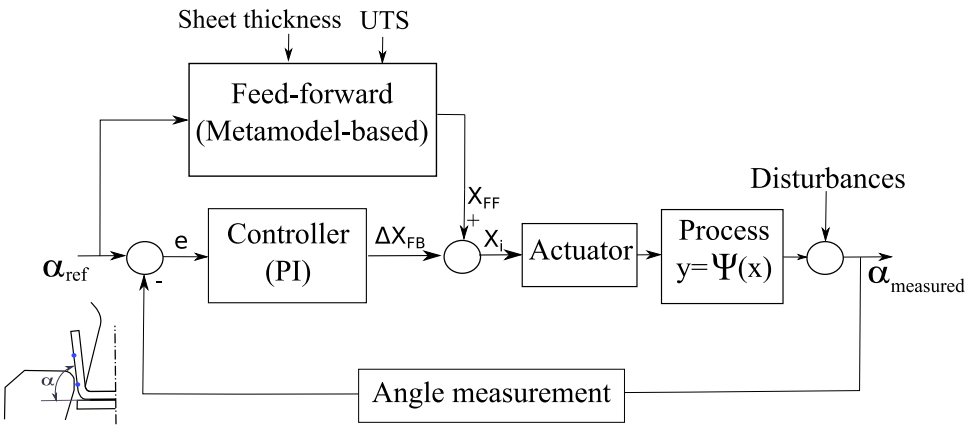

Fig. 11 Feedforward + Feedback (FF + FB) controller

controllers. This concept is referred to as "Disturbances" in Figs. 10 and 11. Disturbances of ±0.25º were set based on the maximum variability observed.

For the tuning of the proportional (K_P) and integral (K_I) gains, a constrained genetic algorithm optimization scheme has been used. The algorithm constraints have been initially defined based on manual tuning during virtual trials to avoid severe overshooting and to achieve robustness and stability. The cost function to be minimized in the optimization problem is given by Eq. (15).

$$minimize \sum_{i=1}^{n} (\alpha_{OBJ} - \alpha_i)^2 \tag{15}$$

where n is the number of the virtually bent parts, α_{OBJ} is the objective bending angle after springback and α_i is the virtually bent angle or the virtual final angle of the formed component. α depends on the press stroke. The press stroke in turn depends on the controller gains as well as the part-to-part and accumulated error, as shown in eqs. (11) and (12) for the FB and FB + FF controllers, respectively.

In order to test the controllers' robustness against possible instabilities, unexpected changes in both UTS and sheet thickness between batches, and also within the same batch, have been emulated for the three controllers. For the FB controller, a stroke far from the optimal one has been chosen to observe how the controller reacts to initial incorrect process settings. For the FF + FB controllers, the stroke is determined by the feedforward term, based on either the numerical or experimental metamodel.

Four different scenarios have been virtually tested, and the controller gains have been tuned to minimize error in Eq. (15), considering these four virtual productions. The main genetic algorithm options used in this work for the three controllers are shown in Table 10.

The controllers' behavior under these virtual production scenarios after error minimization of the controller gains are presented next.

It is important to note that the bend angle values are standardized with respect to the target value. For performance comparisons, the target value represents 0% error. Both the upper and lower limits are considered 100% error relative to the optimum value for evaluating the performance of the controls. Figure 12 illustrates the error calculation procedure for clarity.

In the virtual testing of the controllers, punch stroke adjustments as small as 0.01 mm have been observed. However, this level of precision is not achievable in the real world, as the servomechanical press used can only adjust the punch stroke in increments of 0.05 mm. Therefore, the following criterion has been applied to all controllers tested: if the controller requires a change of less than 0.025 mm, no adjustment is made.

The performance of the three controllers—FB, FB + FF Numerical, and FB + FF Experimental—was evaluated under four virtual scenarios where varying UTS and sheet thickness, shown in Table 11. Table 12 shows the optimized controller gains.

Figure 13 shows the different controller results for the scenarios tested. For each controller, the main highlights are as follows:

FB Controller

The FB controller consistently required multiple parts to stabilize production across all scenarios, often producing out-of-tolerance parts during material changes. As expected, it has no capacity to overcome material changes, with bending angles frequently deviating from optimal values. For instance, in Scenario 1, it produced four out-of-tolerance parts initially, and in Scenario 2, parts showed deviations of up to 58.56% above the optimal angle. While it eventually stabilized, its reliance on feedback led to slower adaptation and higher scrap rates compared to the other controllers.

FB + FF Numerical Controller

The FB + FF Numerical controller demonstrated improved performance, stabilizing after producing fewer out-of-tolerance parts (typically three). It anticipates material changes. While the numerical metamodel captured trends in material and thickness variations well, it lacked precision in predicting the exact punch stroke, requiring corrections by the FB term. This limitation resulted in initial deviations but no

Table 10 Genetic algorithm options for each controller type

Genetic Algorithm Option	FB	FB + FF Numerical	FB + FF Experimental
Population Size	100	100	100
Crossover Fraction	0.8	0.8	0.8
Mutation Options	Gaussian	Gaussian	Gaussian
Selection Function	*selectionstochunif*	*selectionstochunif*	*selectionstochunif*
Max. Generations	1000	1000	1000
Constraints	K_p[0,0.3] K_I [0,0.3]	K_p[0,0.3] K_I [0,0.3]	K_p[0,0.3] K_I [0,0.3]

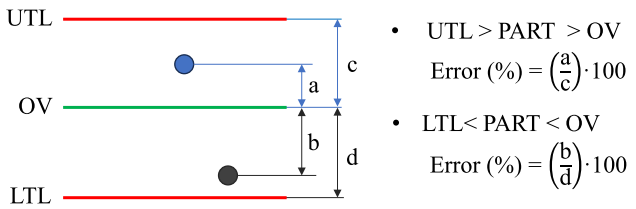

Fig. 12 Schematic of the calculation of the error of the parts. UTL and LTL refer to Upper Tolerance and Lower Tolerance Limit, respectively. OV refers to Objective Value

scrap production once stabilized. It performed consistently across all scenarios, offering a significant improvement over the FB controller. A higher integral gain, relative to the other controllers, is required to ensure the bending angle stays within the acceptable tolerance range. However, this comes with a trade-off, as the higher gain can cause the system some overshooting the target angle.

FB + FF Experimental Controller

The FB + FF Experimental controller outperformed the others, consistently producing only good-quality parts across all scenarios and anticipating material changes. Its experimental metamodel accurately predicted the punch stroke, ensuring optimal bending angles despite variations in UTS and thickness. The controller exhibited exceptional stability, with no scrap or out-of-tolerance parts, even during abrupt material changes or combined property variations. Notably, it proved slightly more sensitive to thickness fluctuations than to UTS changes but maintained optimal production throughout.

Key observations highlight that in the FB controller, a higher K_p was essential for quick responsiveness, though increasing K_I caused instability and overshooting due to the absence of feedforward. In the FB + FF Numerical controller, a high K_I was necessary to compensate for numerical-experimental deviations, maintaining tolerance at the expense of some overshooting, while K_p remained moderate for stability. In contrast, the FB + FF Experimental controller's robust predictions allowed for lower K_p and K_I, ensuring smoother and more stable performance with minimal overshooting. These results underscore the importance of balancing proportional and integral gains based on the predictive accuracy of feedforward models. When predictive accuracy is lower, higher integral gains may be necessary, accepting a trade-off with overshooting. Conversely, when predictive accuracy is higher, lower gains can suffice, leading to smoother operation and greater overall stability. This analysis highlights the value of robust feedforward models in reducing the dependency on feedback corrections and improving system performance.

Table 12 Optimized controller gains for each controller type

Controller Type	Proportional Gain (K_p)	Integral Gain (K_I)
FB	0.0675	7.0608E- 05
FB + FF Numerical	0.0472	0.2942
FB + FF Experimental	0.0218	0.0782

Experimental testing of the new controllers in an industrial environment

Once the controllers have been developed and tuned, the final validation has been conducted using a 400 kN servo-mechanical press and industrial tooling. For this purpose, and considering the available precuts of the five materials, the following trials have been performed:

Firstly, the FB controller has been tested using three of the five different materials. Because the FB controller lacks the ability to predict process changes based on forthcoming material and thickness variations, the materials with the most significant property differences have been selected for the testing campaign. Thus, the controller has been tested with the softest material (CP980 2), followed by the hardest

Table 11 Virtual scenarios for controller tuning. UTS and *t* configurations for each scenario and general observations

Virtual scenario	UTS	t	General observations during material changes
1	Nominal	Nominal	FB: 1 part out-of-tolerances FB + FF Numerical and Experimental: no scrap
2	± 2.5% (random distribution)	Nominal	FB: 2 parts out-of-tolerances FB + FF Numerical and Experimental: no scrap
3	Nominal	± 0.01 mm (random distribution)	FB: 2 parts out-of-tolerances FB + FF Numerical and Experimental: no scrap
4	± 2.5% (random distribution)	± 0.01 mm (random distribution)	FB: 2 parts out-of-tolerances FB + FF Numerical and Experimental: no scrap

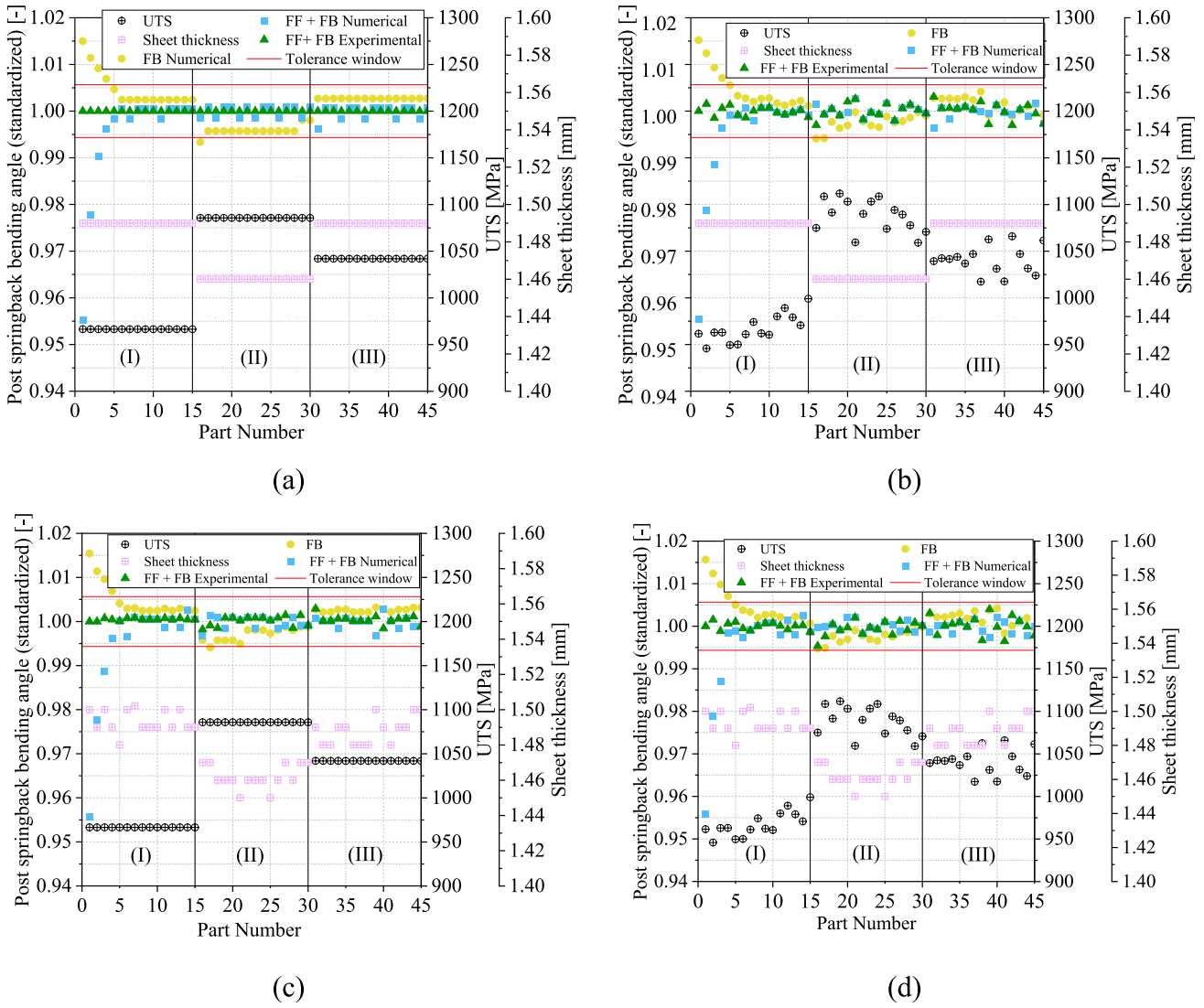

Fig. 13 Bending angle after springback (standardized) for the different virtual productions used for the controller gains optimization. (**a**) Real UTS and thickness values, (**b**) Real thickness values together with ±2.5% change of UTS, (**c**) Real UTS values together with ±0.01 mm change of thickness, (**d**) Both UTS and thickness vary by 2.5% and 0.01 mm, and (**e**) legend of the materials used in the virtual try-outs

(DP980 1), and finally the intermediate one (DP980 3), as in the controllers' virtual tuning tests.

To test the FF + FB controllers, which are generated with both the numerical and the experimental metamodels, a different approach has been selected. This approach has employed the maximum number of materials available, constrained by the amount of precuts provided by the TIER1 company. Consequently, four out of the five materials have been used in the following order: First, the material with the lowest UTS, CP980 2, has been bent. Next, the DP980 2 steel, which has the second highest UTS value, has been processed. Then, DP980 3 steel, having an intermediate UTS value, has been tested. The test campaign has concluded with DP980 1 steel, the hardest of all the materials.

As previously mentioned in the virtual testing, the servo-mechanical press used can only adjust the punch stroke in increments of 0.05 mm. Therefore, the same criterion has

been applied to all controllers tested: if the controller requires a change of less than 0.025 mm, no adjustment is made.

Feedback controller (FB) industrial results

Figure 14a illustrates the industrial performance of the FB controller. In the graph, the experimental bending angles after springback, measured using the springback measuring tool (labelled as Experimental), are shown alongside the theoretical angles predicted by the FB controller (labelled as FB prediction). A virtual try-out of the controller (FB prediction) was performed and compared with the experimental case. In this case, the average UTS for each material and the average sheet thickness per material batch were used, and the same starting stroke as the experimental case was employed. The discrepancies between these values are attributed to process noise, uncontrollable fluctuations, and the limitation of punch stroke adjustment, which cannot be finer than 0.05 mm. Figure 14b shows the experimental and predicted punch stroke for each part produced. Vertical black lines denote material changes, while red lines indicate the product tolerance range.

The testing campaign starts with an arbitrary stroke that is far from the optimum stroke in order to observe the behavior of the controller and to determine the number of parts needed to achieve stable production. After 6 parts, the controller reaches a steady state, while in 4 parts the bend angle after springback error is reduced to a value at which quality parts are produced. On the other hand, it can be observed that the feedback loop is able to reach the target angle despite the uncontrollable disturbances.

After producing 10 parts, when transitioning from CP980 2 to DP980 1 material, it takes two parts to achieve an angle within the specified tolerances. After 20 parts, no scrap is produced, the angle variation being 0.43°. Although stabilized parts are within tolerances, parts 6 to 10 exhibit angles that are 16.14% to 51.30% lower than the target angle. For the DP980 1 material, stabilization results in angles ranging from 7.41% below to 8.21% above the optimum. For the DP980 3 material, after stabilization (part 21), angles range from 33.43% to 67.25% above the optimum.

Feedforward + Feedback (FF+FB) controllers' industrial results

Figure 15a illustrates the industrial performance of the FF + FB controller based on the numerical metamodel. In the graph, the experimental bending angles after springback measured using the bending angle measuring tool (labelled as Experimental), are shown alongside the theoretical angles predicted by the FB controller (labelled as FF + FB Numerical prediction) Fig. 15b shows the experimental

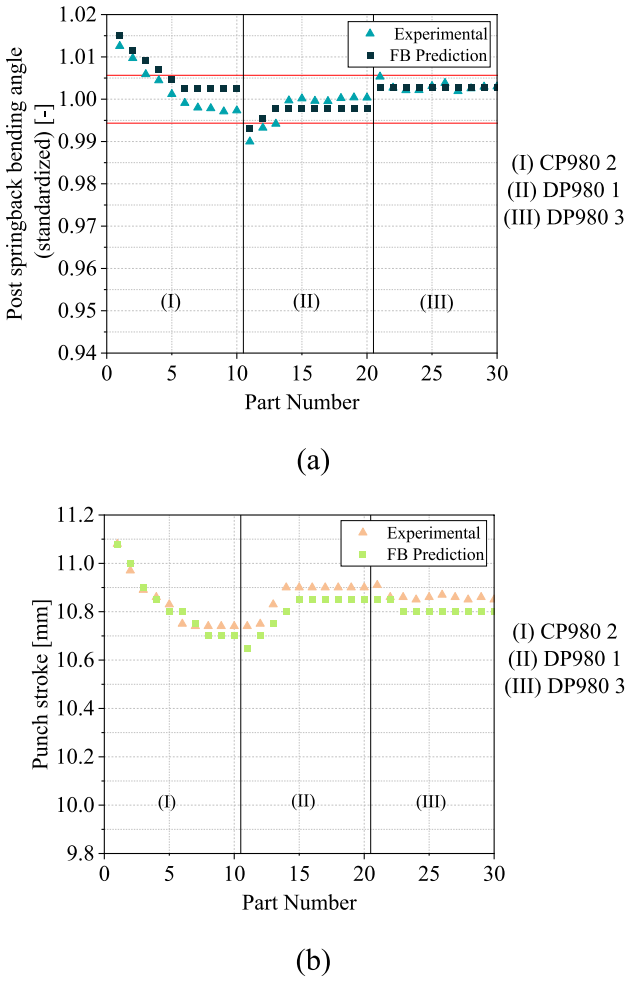

Fig. 14 FB controller results. (**a**) Bending angle after springback (standardized) vs Produced part number and (**b**) Punch stroke vs Produced part number. Vertical black lines indicate material changes while red lines indicate maximum and minimum product tolerances

and predicted punch stroke for each produced part. In the FB + FF Numerical prediction case, a virtual try-out of the control system was performed using the UTS values measured experimentally and the average sheet thickness for each material. In contrast, the Experimental case corresponds to the real production data, using the same UTS values as in the prediction but considering the actual sheet thickness measured for each individual part. Figure 16b shows the experimental and predicted punch stroke for each produced part. Once again, vertical black lines denote material changes, while red lines indicate the product tolerance range

As in the previous case, production begins with a stroke setting that is far from the real optimum, due to the mismatch between the numerical metamodel and the actual process. However, the controller can correct the stroke value in one part, with the second part falling within tolerances. For the CP980 2 material, after stabilization, angles range from

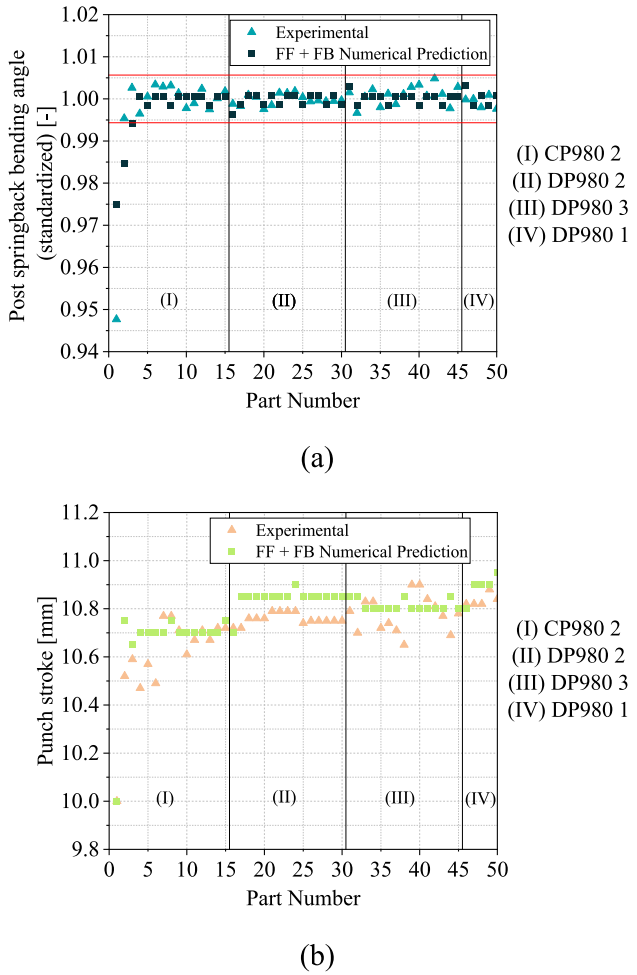

Fig. 15 Feedforward + Feedback Numerical controller (FF + FB Numerical) results. (**a**) Bending angle after springback (standardized) vs Produced part number and (**b**) Punch stroke vs Produced part number. Vertical black lines indicate material changes while red lines indicate maximum and minimum product tolerances

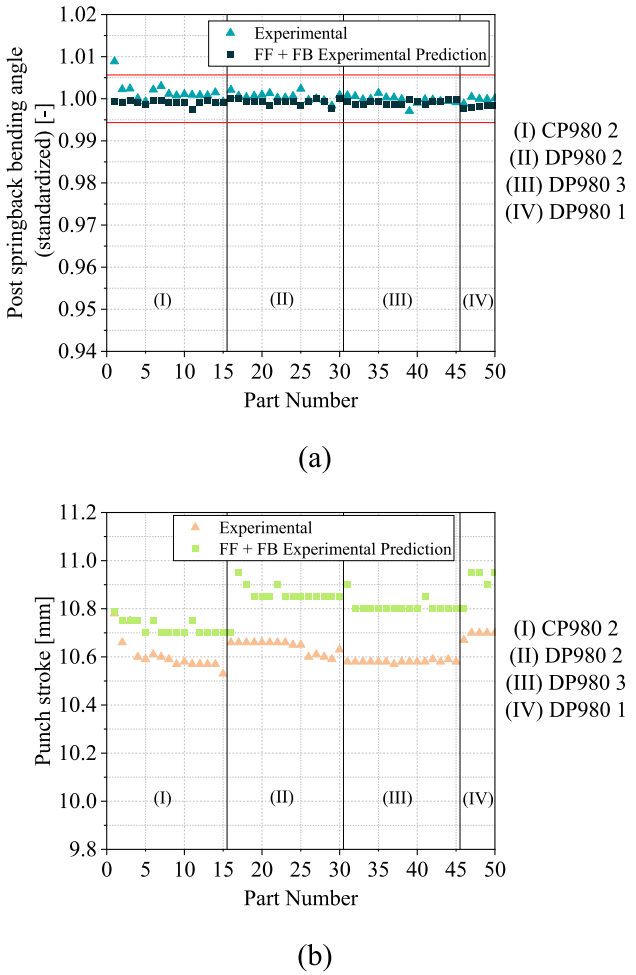

Fig. 16 Feedforward + Feedback Experimental controller (FF + FB Experimental) results. (**a**) Bending angle after springback (standardized) vs Produced part number and (**b**) Punch stroke vs Produced part number. Vertical black lines indicate material changes while red lines indicate maximum and minimum product tolerances

62.3% below to 55.65% above the optimum. The highest variability is observed with the DP980 3 material, where angles range from 58.97% below to 85.47% above the optimum. During production, no scrap was produced due to material changes. Differences between the experimental and predicted press strokes were observed, it could be because the experimental accumulated and part to part error is different from the error of the virtual tryouts. This, together with differences between the nominal thicknesses of each part compared to those measured in the experimental tryouts could be some of the sources of the differences.

Finally, Fig. 16a illustrates the industrial performance of the FF + FB controller based on the experimental metamodel. In the graph, the experimental bending angles after springback, measured using the springback measuring tool (labelled as Experimental), are shown alongside the theoretical angles predicted by the FB controller (labelled as FF + FB Experimental prediction). In the FB + FF Experimental prediction case, a virtual try-out of the control system was performed using the UTS values measured experimentally and the average sheet thickness for each material. In contrast, the Experimental case corresponds to the real production data, using the same UTS values as in the prediction but considering the actual sheet thickness measured for each individual part. Figure 16b shows the experimental and predicted punch stroke for each produced part. Once again, vertical black lines denote material changes, while red lines indicate the product tolerance range.

Only the first component is out of tolerance, probably due to slight changes in tool mounting, and conditions between production runs such as the difference in room temperature between sessions. Note that the FF + FB Experimental training tests were conducted in February,

while the new tests for controller validation were carried out in October under different atmospheric conditions. Additionally, non-controllable fluctuations may also affect the final product geometry. As shown in the graph, the production process is very stable, and after one part, it falls within tolerances and remains near the optimal angle, with a maximum variation of 41.68% from the optimal angle.

As observed in the FF + FB Experimental metamodel, there seems to be an offset between the stroke predicted and the experimental stroke needed in real production (Fig. 16b). To demonstrate this offset, 10 batches of CP980 1 material were tested under the same conditions as the initial tests. Results are shown in Fig. 17, showing a clear offset between the different test sessions. Note that this controller was tested in a separate session, during which the tools were disassembled and reassembled in between the sessions. The PI controller was able to correct this offset.

Discussion

The key discussion points for each tested control type are outlined below:

- FB controller (Fig. 14): This type of control effectively compensated for disturbances in the bending angle and responded to changes in material and thickness. However, it acted only after a defective part was produced, resulting in the generation of defective parts, especially when material changes occurred, and to a lesser extent when thickness changes occurred. This more conservative approach proved inadequate for correcting larger deviations due to its longer response time. Conversely, the strength of the algorithm lies in its reduced sensitivity to measurement noise and variability.
- FF + FB Numerical controller (Fig. 15): Utilizing the feed-forward term allows the material properties and thickness data of the upcoming part to be used in predicting the optimal stroke, preventing scrap due to material changes. This variability could be a result of process fluctuations caused by possible sensor noise during angle measurements and/or variations in material thickness, or from fluctuations in both the process and material. In this scenario, the control is moderately sensitive to changes in thickness. This implies that even minor deviations in sheet thickness can induce angle variations, emphasizing the need for accurate measurement of the parts. Employing a higher integral gain compared to the other two control types can result in some overshooting due to minor variations in thicknesses. This relatively high integral gain was requisite to correcting the offset in the numerical metamodel. In this instance, one part was found to be out of tolerance. This source of variation could be due to variability in the material itself or within part thickness. In this instance, only one part was found to be out of tolerance. This control faced various types of uncertainties, including a modeling error resulting from a numerical metamodel's deviation from the actual process behavior and the inherent disturbances associated with the process, such as material variability and process perturbations. It is important to note that, if the numerical simulation has the same trend as the experimental behavior of the process, it can be sufficient when combined with a feedback control to predict α close to the optimum.
- FF + FB Experimental controller (Fig. 16): This type of control successfully compensated for perturbations and

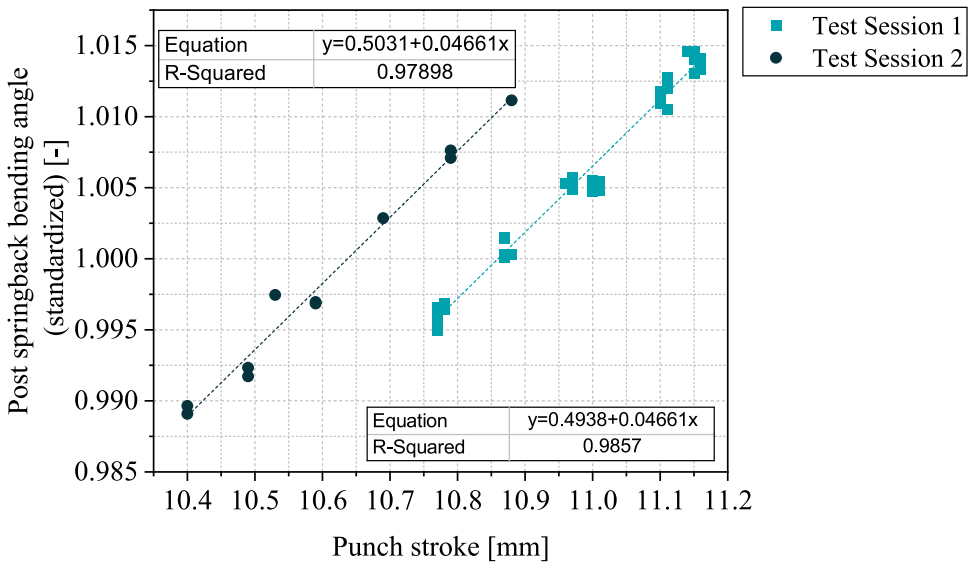

Fig. 17 Differences in bending angle between two different test sessions for CP9801 material

variations in both material and thickness, as well as tool misalignment, achieving bend angles close to the optimum. This effectiveness is likely to be due to the robustness of the experimental metamodel. The substantial size of the experimental dataset and the comprehensive mapping of different sheet thicknesses contributed to the robustness of this control type. In the experiments, only one part was found out of tolerance, at the start, due to the difference in stroke for the same conditions.

It was sufficient to map the process with the production of a reasonable number of parts (in this work 250) to have a virtualized process which can be used to control the production of thousands of parts. What is more, RSM is a polynomial function which is ease-of-use, derivable and understandable, and also execution times are small. This makes it an attractive tool for industry, thus achieving the utilization of a more scientific approach in that area. Part-to-part deviations, which are not covered by the feedforward term, can be corrected with the feedback control.

The calculation of the optimized K_P and K_I by performing an off-line virtual process with the planned material changes and including real process disturbances showed effectiveness in the three controllers. This proved to be a powerful tool, as it can be run in real scheduled production (Fig. 14, Fig. 15, and Fig. 16). For more accurate perturbation values, optimal procedures should involve integrating sensors at strategic locations to monitor machine/tool vibrations, along with incorporating pyrometers within the tool to detect increases in temperature. Temperature has been shown to have a significant effect on the coefficient of friction in forming processes [59–61] and thus on part quality. In fact, room temperature could be one of the factors causing the differences in results between sessions. Therefore, temperature variations during production can affect the bending angle after springback. By utilizing one or more pyrometers, variations in temperature throughout production could be converted into angle variations, provided each part is also measured. These incremental disturbances could then be incorporated into the control scheme to ascertain an optimal punch stroke, while respecting maximum stress in the most critical area of the part—namely, the inner/outer radius.

Table 13 shows the defect rate, the defect rate after control stabilization, and the Root Mean Squared Error (RMSE) calculated for each control type to analyze their performance. The FB controller presents the highest defect rate (30%), while the FF + FB Experimental controller presented a defect rate of 2%. It is important to note that the experimental runs are made with a small number of parts. The defect rate after control stabilization is considered because the starting point of FB controller was chosen arbitrarily, and in this way we can quantify the scrap rate between material changes for the three controllers in isolation. In the latter, disturbances such as the difference in room temperature between sessions and tool reassembly could have affected the offset in press stroke for having the same bend angle. If the defect rate after stabilization of the process is taken into account, the FB controller still shows the highest defect rate (11.11%), while the FF + FB controllers show a rate of 0%. In the case of RMSE, the lowest error is also obtained for the case of control based on experimental data, with an error of 0.16°. The press stroke limitations, acting as actuator disturbances, lead to slight variations in the final bend angle. These variations, sometimes less than 0.025 mm, cannot be achieved due to experimental constraints.

Table 13 Defect rate of each control type., calculated by dividing the number of defective units by the total number of units produced in each case. RMSE was calculated according to Eq. (4), where y in this case is the optimum α and $\mathbf{y}_i^{'}$ is the angle measured/obtained for the i-th part

Control type	Defect rate [%]	Defect rate after stabilization [%]	RMSE [°]
FB controller	30	8	1.06
FF + FB Numerical	2	0	0.68
FF + FB Experimental	2	0	0.16

In summary, each strategy can perform effectively; however, integrating both appears promising. The feedforward approach manages sudden jumps adeptly, while the proportional control effectively addresses part-to-part variations introduced through measurement noise. Although it is well-known that other machine learning algorithms such as ANN provided more accurate results [15], utilizing the Response Surface Methodology in this study proved to be sufficient. It produced accurate bending angles for all tested control strategies, especially when employing a metamodel-based feedforward term to predict the optimal stroke.

Conclusions

In this work, the control of the post-springback bending angle of a seat rail component manufactured by a well-known TIER1 company was performed. Two different types of cold-rolled high-strength steels are used to manufacture this part, therefore resulting in bending angle variability. An enhanced feedback control system and a feedforward control combined with a feedback system were developed and tested experimentally. These control approaches resulted in a more robust manufacturing process, achieving a bending angle within tolerances. The study yielded the following key findings:

- A metamodel based on a finite element model combined with feedback control was used to efficiently achieve a bending angle after springback within tolerances for different materials and part thicknesses. If the metamodel has the same trend, even if there is an offset between the model and reality, it can still be used to control the process, as the feedback loop controller allows adjustment of the metamodel offset to reality based on experimental data. A defect rate of 2% and a RMSE of 0.68° were found for this controller.
- Using feedback control exclusively is not able to anticipate changes in material and/or sheet thickness. With this control an RMSE of 1.06° was obtained. In this case, K_p and K_I are lower compared to the FB + FF controllers. Lower gains often result in smoother transitions between different operating conditions, as the controller responds more gradually to changes. However, increasing the gains could potentially bring more parts within tolerance by enabling faster corrections. However, there is a risk of overshoot, which could lead to instability or parts going beyond the desired specifications.
- A metamodel based on experimental data combined with feedback control provided high robustness to disturbances and abrupt changes in thickness and material properties. Experimental tests were executed successfully, yielding quality parts and achieving a bending angle after springback notably proximate to the optimum. A defect rate of 2% and RMSE of 0.16° were found. However, its robustness is conditioned by other factors such as room temperature or die setup, so a feedback control part is also required.
- The feedforward term determines the necessary press stroke for the thickness and UTS of the subsequent part. By this means, in conjunction with the corrective control from the GA-based optimized controller—considering the error of preceding parts—scrap production is avoided or reduced. The defect rate after stabilization for FF + FB controllers was 0%.
- This work also presents a strategy for programming and tuning specific control gains for planned production. This strategy could dramatically reduce the defect rate.
- Regarding the final industrial implementation, the use of a thickness measurement sensor, such as a laser sensor, is proposed to enable individual sheet measurements, as this approach is both feasible and cost-effective. In contrast, measuring UTS for each part with methods such as eddy current sensors is less practical due to higher costs. Consequently, average UTS values characterized for each material batch were used, which proved sufficient for achieving optimal process control and bending angles despite material variability.

The feedforward + feedback approach markedly reduces scrap compared to straightforward feedback control, which requires a few parts to stabilize and had the highest defect rate and RMSE. Further research will be conducted on control optimization, and control testing in production line will be developed, in which temperature increase of the tools will be taken into account and compensated for, with in-line feedback control.

Acknowledgements This research was funded by the European FLATBEND project, Research for Coal and Steel program, call number RFCS-2017 and proposal number 800730.

Data availability The datasets generated and analyzed during the current study are not publicly available due to confidentiality agreements.

Declarations

Conflict of interest The authors declare that they have no conflict of interest.

References

1. Cullen JM, Allwood JM, Bambach MD (2012) Mapping the global flow of steel: From steelmaking to end-use goods. Environ Sci Technol 46(24):13048–13055. https://doi.org/10.1021/es302433p
2. Cullen JM, Allwood JM (2013) Mapping the global flow of aluminum: From liquid aluminum to end-use goods. Environ Sci Technol 47(7):3057–3064. https://doi.org/10.1021/es304256s
3. Mori K, Akita K, Abe Y (2007) Springback behaviour in bending of ultra-high-strength steel sheets using CNC servo press. Int J Mach Tools Manuf 47(2):321–325. https://doi.org/10.1016/j.ijmachtools.2006.03.013
4. Tekiner Z (2004) An experimental study on the examination of springback of sheet metals with several thicknesses and properties in bending dies. J Mater Process Technol 145(1):109–117. https://doi.org/10.1016/j.jmatprotec.2003.07.005
5. Fei D, Hodgson P (2006) Experimental and numerical studies of springback in air v-bending process for cold rolled TRIP steels. Nucl Eng Des 236(18):1847–1851. https://doi.org/10.1016/j.nucengdes.2006.01.016
6. Ogawa T, Yoshida F (2011) Springback analysis of U-bending with bottoming. AIP Conf Proc 1383:1129–1136. https://doi.org/10.1063/1.3623730
7. Groover MP (2010) Fundamentals of modern manufacturing: materials, processes, ad systems, 4th edn. John Wiley & Sons, Hoboken, NJ, USA
8. Harsch D (2018) "Considering fluctuations of material properties , stainless steel 1 . 4301 , on manufacturability of kitchen sinks,"

IOP Conf Ser Mater Sci Eng https://doi.org/10.1088/1757-899X/418/1/012113.
9. Fischer P, Harsch D, Heingärtner J, Renkci Y, Hora P (2017) A knowledge-based control system for the robust manufacturing of deep drawn parts. Procedia Eng 207:42–47. https://doi.org/10.1016/j.proeng.2017.10.735
10. Harsch D, Heingärtner J, Renkci Y, Hora P (2017) "Influence of scattering material properties on the robustness of deep drawing processes," 10th Forming Technology Forum, no. January 2018.
11. Muñiz L, Trinidad J, Galdos L (2023) Analysis of the mechanical and microstructural fluctuations of high - strength steels and their effect on bending angle. Metals (Basel) 13:1–19. https://doi.org/10.3390/met13091603
12. Viswanathan V, Kinsey B, Cao J (2003) Experimental implementation of neural network springback control for sheet metal forming. J Eng Mater Technol, Trans ASME 125(2):141–147. https://doi.org/10.1115/1.1555652
13. Havinga J, Van Den Boogaard T, Dallinger F, Hora P (2018) Feedforward control of sheet bending based on force measurements. J Manuf Process 31:260–272. https://doi.org/10.1016/j.jmapro.2017.10.011
14. Chatti S, Kleiner M (2014) "Online-Process Control of Air Bending for Thin and Thick Sheet Metal," no. December 2004. https://doi.org/10.1515/JMBM.2004.15.6.455.
15. Vasudevan D, Srinivasan R (2012) Comparison of artificial neural network and response surface methodology in the prediction of springback and bend force in air bending of electrogalvanised steel sheets. In: Proceeding of international conference recent trends in mechanical, instrumentation and thermal engineering
16. Narayanasamy R, Padmanabhan P (2012) Comparison of regression and artificial neural network model for the prediction of springback during air bending process of interstitial free steel sheet. J Intell Manuf 23(3):357–364. https://doi.org/10.1007/s10845-009-0375-6
17. Havinga J, van den Boogaard AH, Dallinger F, Hora P (2014) Inline control of a strip bending process in mass production. In: Proc. Int. deep drawing research group Conf. (IDDRG), pp 1–6
18. Van Den Boogaard T, Havinga J, Van Tijum R (2015) Model-based control of strip bending in mass production. CIRP Ann Manuf Technol 64(1):297–300. https://doi.org/10.1016/j.cirp.2015.04.092
19. Yang M, Manabe KI, Nishimura H (1996) Development of real-time process control system for precision and flexible V-bending with an on-line database. J Mater Process Technol 60(1–4):249–254. https://doi.org/10.1016/0924-0136(96)02338-2
20. Forcellese A, Gabrielli F, Ruffini R (1998) Effect of the training set size on springback control by neural network in an air bending process. J Mater Process Technol 80–81:493–500. https://doi.org/10.1016/S0924-0136(98)00122-8
21. Dilan RA, Balkan T, Platin BE (2017) An online intelligent algorithm pipeline for the elimination of springback effect during sheet metal bending. Procedia Eng 207:1576–1581. https://doi.org/10.1016/j.proeng.2017.10.1081
22. Baseri H, Bakhshi-Jooybari M, Rahmani B (2011) Modeling of spring-back in V-die bending process by using fuzzy learning back-propagation algorithm. Expert Syst Appl 38(7):8894–8900. https://doi.org/10.1016/j.eswa.2011.01.102
23. Fu Z, Mo J (2011) Springback prediction of high-strength sheet metal under air bending forming and tool design based on GA-BPNN. Int J Adv Manuf Technol 53(5–8):473–483. https://doi.org/10.1007/s00170-010-2846-5
24 Alhammadi A, Rafique H, Alkaabi M, Abu Qudeiri J (2018) Experimental investigation of springback in air bending process. IOP Conf Ser Mater Sci Eng 323(1):012021. https://doi.org/10.1088/1757-899X/323/1/012021
25. Miranda SS, Barbosa MR, Santos AD, Pacheco JB, Amaral RL (2018) Forming and springback prediction in press brake air bending combining finite element analysis and neural networks. J Strain Anal Eng Des 53(8):584–601. https://doi.org/10.1177/0309324718798222
26. Havinga J, Klaseboer AHVDBG (2016) "Sequential improvement for robust optimization using an uncertainty measure for radial basis functions," Structural and Multidisciplinary Optimization https://doi.org/10.1007/s00158-016-1572-5.
27. Sunseri M, Cao J, Karafillis AP, Boyce MC (1996) Accommodation of springback error in channel forming using active binder force control: Numerical simulations and experiments. J Eng Mater Technol, Trans ASME 118(3):426–435. https://doi.org/10.1115/1.2806830
28. Hardt DE, Fenn RC (1993) Real-time control of sheet stability during forming. J Manuf Sci E T ASME 115(3):299–308. https://doi.org/10.1115/1.2901664
29. Hsu CW, Ulsoy AG, Demeri MY (2000) An approach for modeling sheet metal forming for process controller design. J Manuf Sci E T ASME 122(4):717–724. https://doi.org/10.1115/1.1286815
30. Hora P, Heingärtner J, Manopulo N, Tong L, Hortig D, Neumann A, Rol K (2011) On the way from an ideal virtual process to the modelling of the real stochastic. In: Proc. forming technology forum (FTF). Zurich, Switzerland, pp 3–14
31. Fischer P, Heingärtner J, Renkci Y, Hora P (2018) Experiences with inline feedback control and data acquisition in deep drawing. Procedia Manuf 15:949–954. https://doi.org/10.1016/j.promfg.2018.07.401
32. Heingärtner J, Veldhuis M, Kott M, Hora P (2020) Process control of forming processes to compensate temperature induced friction changes. Procedia Manuf 47(2019):547–552. https://doi.org/10.1016/j.promfg.2020.04.164
33. Fischer P, Harsch D, Heingartner J, Renkci Y, Hora P (2018) Implementation of feedback control in kitchen sink production. IOP Conf Ser Mater Sci Eng 418(1):012110. https://doi.org/10.1088/1757-899X/418/1/012110
34. Fischer P, Harsch D, Heingärtner J, Renkci Y, Hora P (2017) Approaches for control in deep drawing. In: Proc. forming technology forum (FTF). Enschede, The Netherlands, pp 10–15
35. Manabe K, Yang M, Yoshihara S (1998) Artificial intelligence identification of process parameters and adaptive control system for deep-drawing process. J Mater Process Technol 80–81:421–426. https://doi.org/10.1016/S0924-0136(98)00121-6
36. Cao J, Kinsey B, Solla SA (2000) Consistent and minimal springback using a stepped binder force trajectory and neural network control. J Eng Mater Technol, Trans ASME 122(1):113–118. https://doi.org/10.1115/1.482774
37. Zhao J, Wang F (2005) Parameter identification by neural network for intelligent deep drawing of axisymmetric workpieces. J Mater Process Technol 166(3):387–391. https://doi.org/10.1016/j.jmatprotec.2004.08.020
38. Endelt B, Tommerup S, Danckert J (2013) A novel feedback control system - Controlling the material flow in deep drawing using distributed blank-holder force. J Mater Process Technol 213(1):36–50. https://doi.org/10.1016/j.jmatprotec.2012.08.003
39. Khadra FA, Abu Qudiri JE, Hussein HMA (2014) Prediction the springback in air-bending process using neural network metamodel. Appl Mechanics Mater 619:3–7. https://doi.org/10.4028/www.scientific.net/AMM.619.3
40. El Mrabti I, Touache A, El Hakimi A, Chamat A (2021) Springback optimization of deep drawing process based on FEM-ANN-PSO strategy. Struct Multidiscip Optim 64(1):321–333. https://doi.org/10.1007/s00158-021-02861-y
41. Kim H, Nargundkar N, Altan T (2007) Prediction of Bend Allowance and Springback in Air Bending. J Manuf Sci Eng 129(April):2016. https://doi.org/10.1115/1.2673527

42. Elkins KL, Sturges RH (1999) Springback analysis and control in small radius air bending. J Manuf Sci E T ASME 121(4):679–688. https://doi.org/10.1115/1.2833103
43. De Vin LJ (2000) Curvature prediction in air bending of metal sheet. J Mater Process Technol 100(1):257–261. https://doi.org/10.1016/S0924-0136(99)00489-6
44. Khadra FA, El-Morsy A-W (2016) Prediction of Springback in the Air Bending Process Using a Kriging Metamodel. Technology & Applied Science Research 6(5):1200–1206
45. Molitor DA, Arne V, Kubik C, Noemark G, Groche P (2024) "Inline closed-loop control of bending angles with machine learning supported springback compensation," Int J Mater Forming 17(1) https://doi.org/10.1007/s12289-023-01802-y
46. Thipprakmas S, Phanitwong W (2011) Process parameter design of spring-back and spring-go in V-bending process using Taguchi technique. Mater Des 32(8–9):4430–4436. https://doi.org/10.1016/j.matdes.2011.03.069
47. Panda N, Pawar RS (2018) Optimization of process parameters affecting on spring-back in V-bending process for high strength low alloy steel HSLA 420 using FEA (HyperForm). Int J Aerospace Mech Eng 12(1):28–34
48. Kaps L, Lipowski HJ, Meywerk M, Werner H, Scholz S-P (1999) Auswerteverfahren zur Weiterverarbeitung von Versuchsdaten. Internal communication, VDEh Working Group, Düsseldorf, Germany
49. Agirre J, Galdos L, Saenz de Argandoña E, Mendiguren J (2018) Hardening prediction of diverse materials using the Digital Image Correlation technique. Mech Mater 124(January):71–79. https://doi.org/10.1016/j.mechmat.2018.05.007
50. Banabic D (2016) Sheet metal forming processes, 53(9) https://doi.org/10.1017/CBO9781107415324.004.
51. Hockett JE, Sherby OD (1975) Large strain deformation of polycrystalline metals at low homologous temperatures. J Mech Phys Solids 23(2):87–98. https://doi.org/10.1016/0022-5096(75)90018-6
52. Muñiz L, Trinidad J, Garcia E, Peinado I, Montes N, Galdos L (2023) On the use of advanced friction models for the simulation of an industrial stamping process including the analysis of material and lubricant fluctuations. Lubricants 11(5):193. https://doi.org/10.3390/lubricants11050193
53. Filzek J, Ludwig M, Groche P (2011) Improved FEM simulation of sheet metal forming with friction modelling using laboratory tests. In: Proc. Int. Deep DRawing Research Group Conf. (IDDRG). Bilbao, Spain
54. Garud SS, Karimi IA, Kraft M (2017) Design of computer experiments: A review. Comput Chem Eng 106:71–95. https://doi.org/10.1016/j.compchemeng.2017.05.010
55. Durakovic B (2018) "Design of Experiments Application , Concepts , Examples : State of the Art," no. December 2017 https://doi.org/10.21533/pen.v5i3.145
56. Myers RH, Montgomery DC, Anderson-Cook CM (2016) Response surface methodology: process and product optimization using designed experiments, 4th edn. John Wiley & Sons, Hoboken, NJ, USA
57. Simpson TW, Peplinski JD, Koch PN, Allen JK (2001) Metamodels for computer-based engineering design: survey and recommendations. Eng Comput 17:129–150. https://doi.org/10.1007/PL00007198
58. Jackson EK, Roberts W, Nelsen B, Williams GP, Nelson EJ, Ames DP (2019) Introductory overview: Error metrics for hydrologic modelling – A review of common practices and an open source library to facilitate use and adoption. Environ Model Softw 119(May):32–48. https://doi.org/10.1016/j.envsoft.2019.05.001
59. Waanders D, Marangalou JH, Kott M, Gastebois S, Hol J (2020) Temperature dependent friction modelling: The influence of temperature on product quality. Procedia Manuf 47(2019):535–540. https://doi.org/10.1016/j.promfg.2020.04.159
60. Kott M, Erz C, Heingärtner J, Groche P (2020) Controllability of temperature induced friction effects during deep drawing of car body parts with high drawing depths in series production. Procedia Manuf 47(2019):553–560. https://doi.org/10.1016/j.promfg.2020.04.166
61. Filzek J, Keil D, Schröder H (2021) Temperature induced friction increase in friction test and forming demonstrator for sheet metal forming. In: Proc. 24th European scientific association for material forming (ESAFORM 2021). Liège, Belgium, pp 1–10